Biosensors and Bioelectronics 79 (2016) 1–8

Contents lists available at ScienceDirect

Biosensors and Bioelectronics

journal homepage: www.elsevier.com/locate/bios

High-yield synthesis of strong photoluminescent N-doped carbon nanodots derived from hydrosoluble chitosan for mercury ion sensing via smartphone APP

Lei Wang [a], Baoqiang Li [a,*], Feng Xu [b,c], Xinyao Shi [a], Demeng Feng [a], Daqing Wei [a], Ying Li [d], Yujie Feng [a], Yaming Wang [a], Dechang Jia [a], Yu Zhou [a]

[a] Institute for Advanced Ceramics; State Key Laboratory of Urban Water Resource and Environment, Harbin Institute of Technology, Harbin 150001, PR China
[b] MOE Key Laboratory of Biomedical Information Engineering, School of Life Science and Technology, Xi'an Jiaotong University, Xi'an 710049, PR China
[c] Bioinspired Engineering and Biomechanics Center (BEBC), Xi'an Jiaotong University, Xi'an 710049, PR China
[d] Sino-Russian Institute of Hard Tissue Development and Regeneration, the Second Affiliated Hospital of Harbin Medical University, Harbin 150001, PR China

ARTICLE INFO

Article history:
Received 16 September 2015
Received in revised form
16 November 2015
Accepted 27 November 2015
Available online 4 December 2015

Keywords:
Nitrogen-doped carbon nanodots
Nitrogen-containing biomass
High-yield synthesis
Smartphone-based mercury ion sensor

ABSTRACT

Photoluminescent carbon nanodots (CNDs) have offered considerable potential to be used in biomedical and environmental fields including live cell imaging and heavy metal ion detection due to their superior quantum emission efficiencies, ability to be functionalized using a variety of chemistries and apparent absence of toxicity. However, to date, synthetic yield of CNDs derived from biomass via hydrothermal carbonization is quite low. We report here the synthesis of nitrogen-doped carbon nanodots (N-doped CNDs) derived from hydrosoluble chitosan via hydrothermal carbonization. The synthetic yield could reach 38.4% which is 2.2–320 times increase compared with that from other biomass reported so far. These N-doped CNDs exhibited a high quantum yield (31.8%) as a consequence of nitrogen incorporation coincident with multiple types of functional groups (C=O, O–H, COOH, and NH_2). We further demonstrate applications of N-doped CNDs as probes for live cell multicolor imaging and heavy metal ion detection. The N-doped CNDs offered potential as mercury ion sensors with detection limit of 80 nM. A smartphone application (APP) based on N-doped CNDs was developed for the first time providing a portable and low cost detection platform for detection of Hg^{2+} and alert of heavy metal ions contamination.

1. Introduction

Carbon nanodots (CNDs), novel zero-dimensional carbon nanomaterials, have attracted in-creasing attention owing to their intriguing luminescent properties, good solubility, high chemical stability and excellent biocompatibility compared with traditional semiconductor quantum dots (*e.g.,* CdSe and ZnSe) (Gao et al., 2015; Hu et al., 2015; Jiang et al., 2015). CNDs can be synthesized from a variety of carbon sources including graphene (Li et al., 2012), small organic molecules (Dong et al., 2013) and biomass (Zhang et al., 2015; Zhu et al., 2012). Recent research suggests that they offer promise as alternative probes for bioimaging (Guo et al., 2013; Sun et al., 2013) and as biosensors (Gu et al., 2015; Zheng et al., 2015). Among these various carbon sources, biomass has attracted special attention due to the diversity, renewability and low cost. CNDs derived from various biomass sources have been reported, including food-waste (Park et al., 2014), green tea (Hsu et al., 2013), orange juice (Sahu et al., 2012), egg white/yolk (Wang et al., 2012) and coffee grounds (Hsu et al., 2012). However, low-yield synthesis and low quantum yield (QY) of CNDs derived from biomass limits their practical large-scale applications. High-yield CND synthesis with greatly improved QY provides significant impetus for the current studies. Furthermore, the potential for large-scale synthesis of CNDs from biomass provides an additional economic motivation for practical applications (*e.g.* low-cost commercial probes for bioimaging and optoelectronic devices).

Recently interest has targeted the synthesis of heteroatom-doped CNDs, especially nitrogen-doped CNDs (N-doped CNDs) (Ma et al., 2012; Zhang et al., 2012), because N-doped CNDs appear to offer improved QY. Nitrogen doping is thought to facilitate electron transfer and restrain non-radiative decay processes (Xu et al., 2013). Also, N-doped CNDs offer surface reaction activity for covalent linkage of functional pendant, such as receptors capable of selectively detecting cancer cells (Song et al., 2012). Furthermore, N-doped CNDs exhibit high selectivity and specificity for the detection of metal ions owing to their strong affinity with amino groups (Barati et al., 2015), making them for sensitive and selective

* Corresponding author.
E-mail address: libq@hit.edu.cn (B. Li).

http://dx.doi.org/10.1016/j.bios.2015.11.085
0956-5663/

detection of metal ions.

Low concentrations of Hg^{2+} have traditionally been detected using spectroscopic methods including atomic absorption spectroscopy (AAS), inductively coupled plasma mass spectrometry (ICP-MS) and atomic fluorescence spectrometry (AFS). However, these approaches require bulk and expensive instruments. Therefore, there is an urgent need for portable and cost-effective Hg^{2+} detection that could be conducted on laptop/smartphone based on MATLAB code/APP.

Chitosan is a biocompatible natural polymer biomaterial with unique amino groups that could serve as source of N-doped CNDs. The use of hydrosoluble chitosan can offer high-yield synthesis, and the nitrogen element was transferred into N-doped CNDs for high QY. Thus, a route for large-scale synthesis of N-doped CNDs with high-yield synthesis and high QY are demanded.

In this work, N-doped CNDs derived from hydrosoluble chitosan were synthesized with high-yield synthesis ($38.4 \pm 3.4\%$) and high QY (31.8%). High selective and sensitive Hg^{2+} detection was demonstrated by photoluminescence quenching. Colorimetric measurement was presented by using MATLAB code and smartphone APP potentially for portable and cost-effective Hg^{2+} sensors. The practical use for Hg^{2+} determination in river water was also explored by sensitive PL spectrum and portable imaging analysis using MATLAB code and smartphone APP respectively.

2. Experimental section

2.1. Chemicals and materials

Chitosan ($M\eta = 3.4 \times 10^5$, degree of deacetylation = 91%) and methacrylic anhydride was purchased from Adamas-beta. Deionized water (Millipore Milli-Q grade) with resistivity of 18.2 MΩ was used in all experiments. Dialysis bag (retained molecular weight 1000 Da) was supplied by Solarbio. Dulbecco's modified Eagle's medium (DMEM), 3-(4,5-dimethylthiazol-2-yl)-2,5-diphenyltetrazolium bromide (MTT), and fetal bovine serum were purchased from Gibco (Life Technologies).

2.2. High-yield synthesis of N-doped CNDs from hydrosoluble chitosan

Hydrosoluble chitosan was synthesized according to our previous work (Li et al., 2015) and was dissolved in deionized water. The 1 mg/mL solution was sealed into a Teflon autoclave, which was put into an oven at 220 °C for 12 h. The obtained dark brown solution was centrifuged (8000 rpm, 30 min) and filtered (membrane of 220 nm) to remove agglomerated deposit. N-doped CNDs powder was obtained by dialyzing against ethanol (50%) and deionized water (replacing fresh ethanol solution or deionized water per 6 h) respectively for 2 days followed by lyophilization, which was then accurately quantified to an aqueous solution of 10 mg/mL as stock solution. The synthetic yield (SY) was determined according to the following Eq. (1):

$$SY = \frac{M_{CNDs}}{M_{HC}} \times 100\% \quad (1)$$

Where SY is the synthetic yield, M_{CNDs} and M_{HC} are the mass of as-prepared N-doped CNDs and hydrosoluble chitosan, respectively.

2.3. Sensitive and portable detection of Hg^{2+} via PL spectrum, MATLAB code and smartphone APP

The selectivity and specificity of N-doped CNDs were examined using interfering metal ions such as Cd^{2+}, Co^{2+}, Ca^{2+}, Cu^{2+}, Mg^{2+}, Mn^{2+}, Ni^{2+}, Pb^{2+}, Sr^{2+}, Zn^{2+}, Al^{3+} and Ag^{+}. The concentrations of Hg^{2+} and interfering metal ions were all 300 μM. To study the interference, N-doped CNDs solution was mixed with Hg^{2+} in the absence and presence of other interfering metal ions at concentrations of eight times that of Hg^{2+}. The fluorescence spectra were recorded after equilibrating for 10 min.

The sensibility detection of Hg^{2+} using PL spectrum was performed in phosphate-buffered saline (PBS) solution buffer solution. In a typical experiment, 40 μL of N-doped CNDs stock solution was mixed with 4 mL of water. Then, 50 μL of different concentration of Hg^{2+} was added, and equilibrated for 10 min before PL measurement. PL emission spectra were recorded at excitation wavelength of 360 nm. All measurements were conducted by triple samples at room temperature.

Colorimetric detection of Hg^{2+} was performed using a relative grayscale change of fluorescent images. Typically, 0.5 μL of N-doped CNDs solution with different concentrations of Hg^{2+} was placed as a single drop on a slide glass. The drop was imaged using fluorescence microscope. The MATLAB code automatically analyzes the region of interest (ROI) providing a mean optical density (MOD). A quantitative relationship between MOD_0/MOD-1 and Hg^{2+} concentration was fit to obtain the following Eq. (2):

$$Y = 0.0265X - 0.0051 \quad (2)$$

Where Y is value of MOD_0/MOD-1; and MOD_0 and MOD are mean optical densities of images in the absence and presence of Hg^{2+} respectively; X is the Hg^{2+} concentration.

Colorimetric detection of Hg^{2+} using smartphone was performed based on smartphone application (**Colorimetric Analysis**). The captured images were analyzed in digitally separated green channels to obtain average intensity (AI) of ROI. The AI was analyzed and displayed on screen of smartphone. A quantitative relationship between AI_0/AI-1 and Hg^{2+} concentration was fit to obtain the following Eq. (3):

$$Y = 0.0203X + 0.0484 \quad (3)$$

Where Y is value of AI_0/AI-1; and AI_0 and AI average intensity of ROI in the absence and presence of Hg^{2+} respectively; X is the Hg^{2+} concentration.

Standard addition method was used to evaluate the feasibility of N-doped CNDs solution for determination of Hg^{2+} in river (Songhua River, Harbin). River water were collected and filtered through a 0.22 μm membrane. The resultant river water with different concentrations of Hg^{2+} was spiked with N-doped CNDs stock solution. Colorimetric assay of Hg^{2+} based on smartphone was conducted by Colorimetric Analysis APP. The contaminated river water was also analyzed by ICP-AES for determining Hg^{2+} as standard concentration.

2.4. Statistical analysis

Every analysis was run at least three times. All data were expressed as mean ± SD. Statistically significant differences were evaluated using Student's T-test.

3. Results and discussion

3.1. High-yield synthesis of N-doped CNDs

Chitosan is a feasible and cheap biomass with unique amino groups, and it was served as carbon and nitrogen source for synthesis of N-doped CNDs by hydrothermal method. The use of hydrosoluble chitosan provides high-yield synthesis and synchronously the nitrogen element is transferred into the CNDs for a

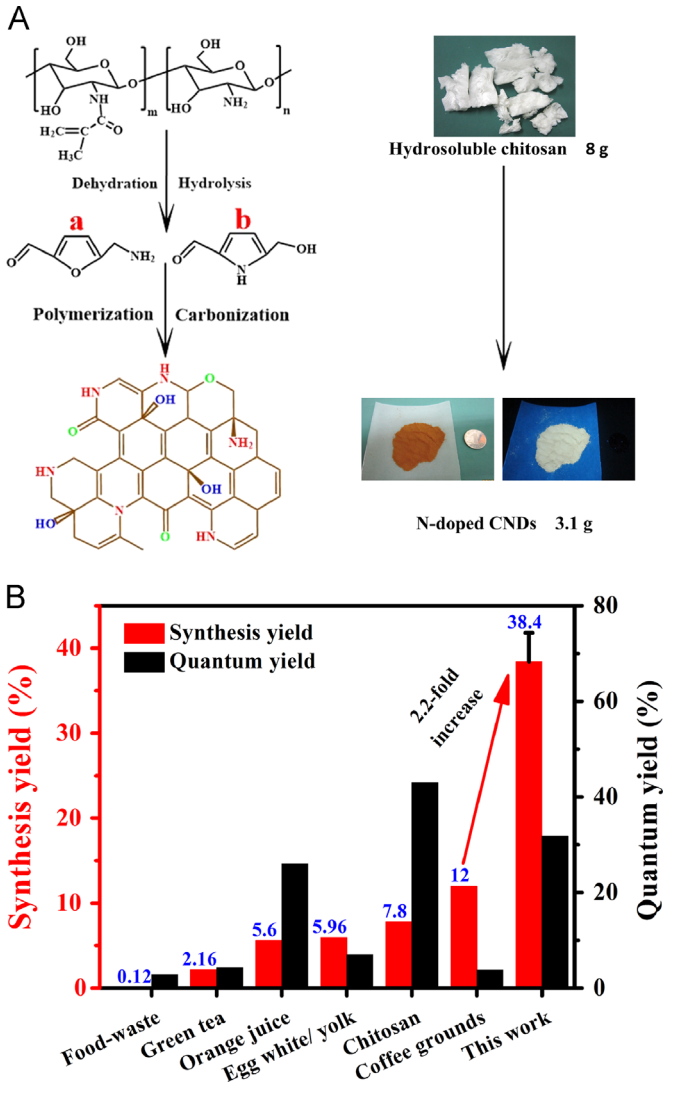

Fig. 1. High-yield synthesis of N-doped CNDs derived from hydrosoluble chitosan. (A) Schematic presentation for high-yield synthesis of N-doped CNDs from 8.0 g hydrosoluble chitosan; Approximate 3.1 g N-doped CNDs powder under day light and UV light at 365 nm with a 1 CNY coin; (B) Synthetic yield and quantum yield of CNDs derived from various biomass.

high QY. The possible synthesis route of N-doped CNDs is postulated based on the previous work. (1) Hydrolysis, dehydration and decomposition of 2-amino-2-deoxy-β-D-glycopyranose results in soluble compounds like furfural (a), pyrrole (b), and other few organic molecule (Fig. 1A); (2) polymerization and carbonization of the products (a, b) formed in step1; (3) nucleation and growth of carbon substances; (4) oxidation of grown carbon substances (Falco et al., 2011). The hydrosoluble chitosan (8 g) converted into gram-scale solid N-doped CNDs powder (3.1 g). Various biomass have been used to synthesize CNDs, such as food-waste, green tea and orange juice. However, the synthetic yield from these sources ranges from 0.12% to 12%. Indeed the yield of N-doped CNDs from chitosan is comparatively low (9.4%) partially due to its poor solubility in water. In contrast, the yield from hydrosoluble chitosan reaches 38.4 ± 3.4%, which is impressive 2.2–320 times increase (Fig. 1B). The QY of N-doped CNDs (31.8%) (Table S1) is higher than CNDs from other biomass (typically < 10%). The yield of N-doped CNDs is much higher than previously reported other CNDs compared with other carbon sources (Table S2). The QY of N-doped CNDs still have the advantage of high value among these carbon sources including small molecule, graphene oxide, and activated carbon. The incorporation of nitrogen element benefits the higher QY (Xu et al., 2013). All these results indicate that our approach may provide an efficient route for large-scale synthesis of high QY N-doped CNDs.

3.2. Optical, morphology and surface properties of N-doped CNDs

As illustrated in Fig. 2A, the N-doped CNDs absorption spectrum exhibited a peak at 289 nm, a typical absorption of $\pi \rightarrow \pi^*$ electronic transition of aromatic π system or $n \rightarrow \pi^*$ electronic transition of carbonyl groups. The well-dispersed aqueous solution of N-doped CNDs exhibited transparent and slight yellow and showed bright blue luminescence under UV (inset in Fig. 2A). The PL emission shifts to longer wavelength with increasing excitation from 280 to 450 nm (Fig. 2B). The red shift in emission peak positions with different excitation wavelengths arose not only from different sizes of N-doped CNDs, but also primarily from different emissive sites on N-doped CNDs (Sun et al., 2006). The average size is 3.8 ± 1.2 nm as reflected by HRTEM images (Figs. 2C and S1). Furthermore, the magnified HRTEM image shows a crystalline structure with lattice spacing of 0.22 nm which may be attributable to (102) facet of graphitic (sp^2) carbon. Fast Fourier transform (Fig. S2) reveals the characteristic hexagonal diffraction pattern of graphite, further supporting the formation of graphitic structure. The G band at 1569 cm^{-1} is related to sp^2-bonded carbon atoms in the 2D hexagonal lattice of a graphite cluster. The D band at 1354 cm^{-1} is assigned to carbon atoms in the disordered carbon structure (Fig. S3).

Three dominant peaks at 285, 399 and 532 eV of XPS survey spectrum were ascribed to C1s, N1s and O1s (Fig. S4). The elemental analysis indicated that the composition of N-doped CNDs was C 59.49 wt%, N 6.32 wt%, H 5.78 wt% and O (calculated) 28.41 wt% (Table S3). The carbon element of N-doped CNDs obviously increased as high as 29% with the loss of hydrogen and oxygen during carbonization. The XPS spectrum of N_{1s} core electrons exhibits three fitted peaks at 398.5 (blue), 399.7 (green) and 401.3 (red) eV, which are associated with N in a graphite-like structure ($N\text{-}C_3$), pyridinic-like N, and N–H bond of NH_2 groups, respectively (Liang et al., 2013). Their relative contents are *ca.* 10%, 67% and 23% respectively on the basis of calculations of the integral area as marked in Fig. 2D. The FTIR spectrum (Fig. S5) shows a new peak at 1717 cm^{-1} and three peaks at 3325, 2924, and 1607 cm^{-1}, which correspond to C=O, O–H, CH_2 and NH_2, respectively.

3.3. Cell multicolor bioimaging

Fig. 3A shows cell viability with N-doped CNDs of 35, 70, 122.5, 175, 280 and 490 μg/mL for 24, 36 and 72 h. The cell viability at all concentrations maintains above 85% even at 72 h. In addition, no statistically significant differences (marked by "NS") were observed between N-doped CNDs (70 μg/mL) and a control group, which indicates that N-doped CNDs exhibit low cytotoxicity and better biocompatibility, potentially valuable for live cell imaging and tracking. As depicted in Fig. 3B, cell uptake was clearly observed via fluorescence and bright field after incubation with 70 μg/mL N-doped CNDs for 3 h. Bright blue (360–380 nm) and green (460–490 nm) fluorescence of the HCT116 cells were observed. No autofluorescence emerges from cells in fluorescence field (Fig. S6). We also found the bright fluorescent areas agglomerating in cytoplasmic areas of HCT116 cells, whereas only weak fluorescence is observed in regions near and in the nuclei.

3.4. Sensitive detection of Hg^{2+} based on PL spectrum

To explore the feasibility of the N-doped CNDs for Hg^{2+} detection, changes in PL intensity were studied in the presence and

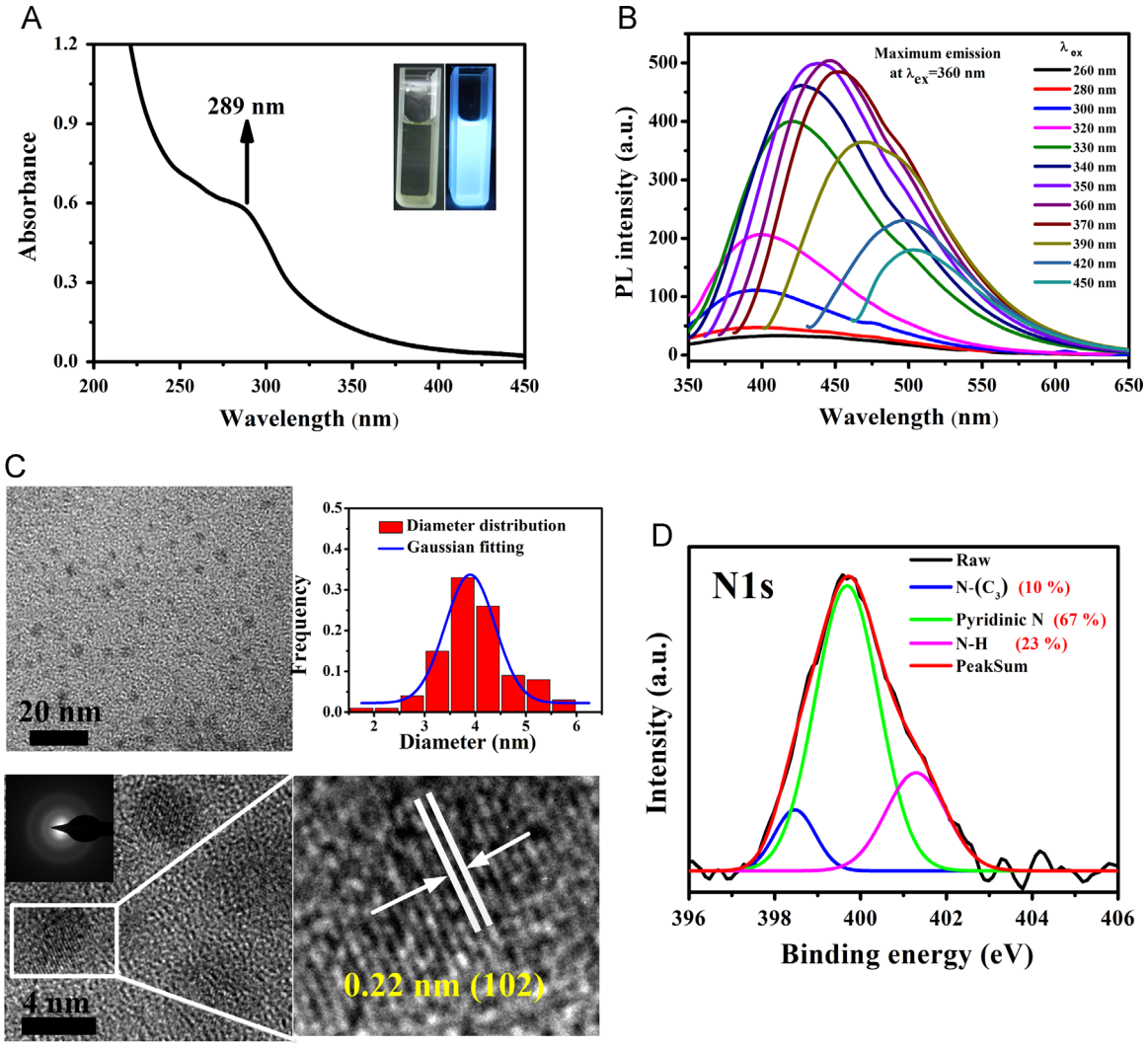

Fig. 2. Optical, Morphology and surface properties of N-doped CNDs. (A) UV–vis absorbance spectrum of N-doped CNDs diluted suspension. Inset shows images of suspension under day light (left) and UV light at 365 nm (right); (B) the excitation-dependent photoluminescence spectra of N-doped CNDs under different excitation wavelengths; (C) TEM images of the N-doped CNDs with size distribution histogram (3.8 ± 1.2 nm). High-resolution TEM images of N-doped CNDs with inset of SAED patterns; (D) XPS high resolutions scan of the N_{1s}. (For interpretation of the references to color in this figure, the reader is referred to the web version of this article.)

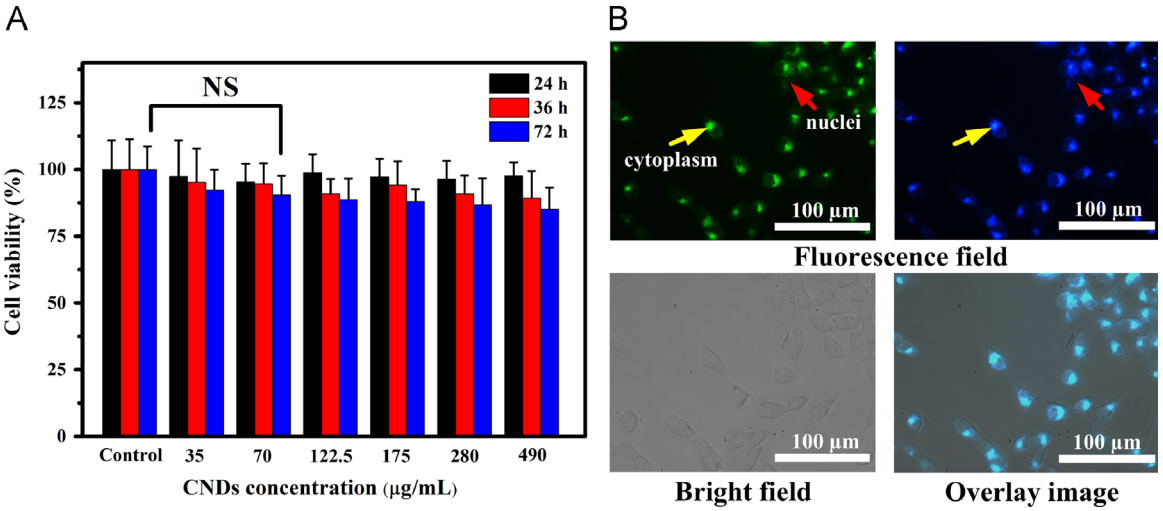

Fig. 3. N-doped CNDs for live cell multicolor bioimaging. (A) Cell viability of HCT116 human cancer cells after incubation with different concentrations N-doped CNDs for 24, 36 and 48 h by MTT assay. (B) Fluorescence images of HCT116 cells treated with N-doped CNDs under 360–380 nm, 460–490 nm excitation, bright field and overlay image. (For interpretation of the references to color in this figure, the reader is referred to the web version of this article.)

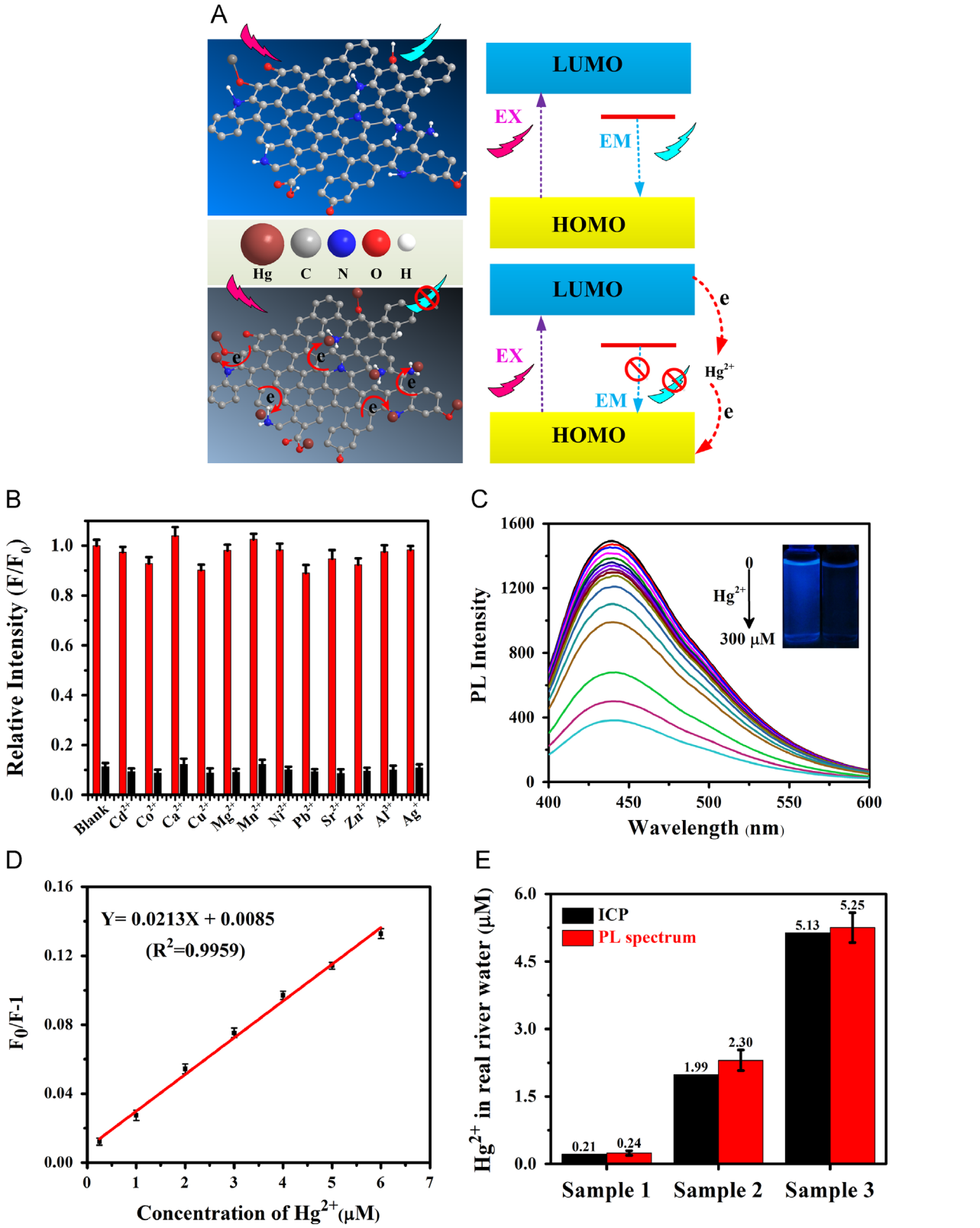

Fig. 4. Sensitive mercury ion sensing based on PL spectrum. (A) The proposed FL quenching mechanism for N-doped CNDs/Hg^{2+} system; (B) the relative fluorescence intensities (F/F_0) of N-doped CNDs in the presence of metal ions (300 μM), and following treatment of the mixture solution with 300.0 μM Hg^{2+}; (C) representative PL emission with increasing Hg^{2+} concentrations (0~300 μM), the inset displays photographs with Hg^{2+} concentrations of 0 and 300 μM; (D) the dependence of $(F_0/F)-1$ on concentrations of Hg^{2+}; (E) Hg^{2+} concentration in river water measured by PL spectrum (red) and using ICP-AES (black). (For interpretation of the references to color in this figure legend, the reader is referred to the web version of this article.)

absence of Hg^{2+}. N-doped CNDs solution exhibits strong fluorescence at 440 nm in the absence of Hg^{2+}. In contrast, the presence of Hg^{2+} leads to a significant decrease of intensity, indicating that Hg^{2+} could quench fluorescence and N-doped CNDs are favorable to sensitive Hg^{2+} detection (Zhou et al., 2012). The PL emission of CNDs derives from the radiative recombination of excitons, which could be quenched by metal ions such as Hg^{2+} via nonradiative electron-transfer between CNDs and metal ions (Zhu et al., 2013). As shown in Fig. 4A, it exist some oxygen/nitrogen functional groups on surface of N-doped CNDs, which can coordinate with Hg^{2+} to form complexes (Liu et al., 2013), leading to the transfer of electron from N-doped CNDs to Hg^{2+}. The introduction of N into the graphitic-like N-doped CNDs should effectively tune the electronic density of N-doped CNDs which would promote the coordination interaction between oxygen functional groups on the edge of N-doped CNDs and Hg^{2+}. The fast electron transfer process and promoted interaction, therefore, causes significant FL quenching of N-doped CNDs system.

To estimate the selectivity and specificity of N-doped CNDs as a fluorescent probe, PL intensities were analyzed in the presence of metal ions at a concentration of 300.0 μM (Fig. 4B). The PL intensity of N-doped CNDs is strongly quenched (80% attenuation) in the case of Hg^{2+}. Based on this phenomenon, N-doped CNDs offer potential to selectively detect Hg^{2+} in the presence of other metal ions at concentrations of 300 μM. We found that the tolerance concentrations of Co^{2+}, Cu^{2+} and Pb^{2+} when sensing Hg^{2+} using N-doped CNDs were at least 8 times Hg^{2+} concentrations (Fig. S7). For sensitivity tests, PL intensity upon adding different concentrations of Hg^{2+} ranging from 0 to 300 μM was monitored. As shown in Fig. 4C, the PL intensity of N-doped CNDs shows a gradual decrease with increasing Hg^{2+} concentration, revealing that sensing is sensitive to Hg^{2+}. Two good linear relationships (0.25–6 and 80–300 μM) exist between PL intensity and Hg^{2+} concentration in Fig. S8. At low concentrations (Fig. 4D) it fits the linear Stern-Volmer equation, illustrating a photophysical process by a single reaction (static quenching Fig. 4A). The detection limit is as low as 80 nM (16 ppb, parts per billion) at signal-to-noise ratio (*S*/*N*) of 3. It should be noted that our Hg^{2+} detection limit is much lower than previously reported other CNDs (Table S4), and lower than the maximum allowable Hg^{2+} discharge of 50 ppb according to the Chinese Integrated Wastewater Discharge Standard of the second category pollution (GB 8978-1996). The high QY (31.8%) is higher than that previously reported sensor; and it was fascinating especially considering without passivation, favorable for sensitive Hg^{2+} detection. The practical assay for Hg^{2+} determination in water sample was explored by using contaminated river water containing different concentrations of Hg^{2+}. The Hg^{2+} concentrations determined using a fitting curve match well with the standard concentrations of contaminated river water with a slight increase (2–15%), Fig. 5E and Fig. S9. Despite potential interference from numerous metal ions and organics existing in river water, the N-doped CNDs sensor could still distinguish

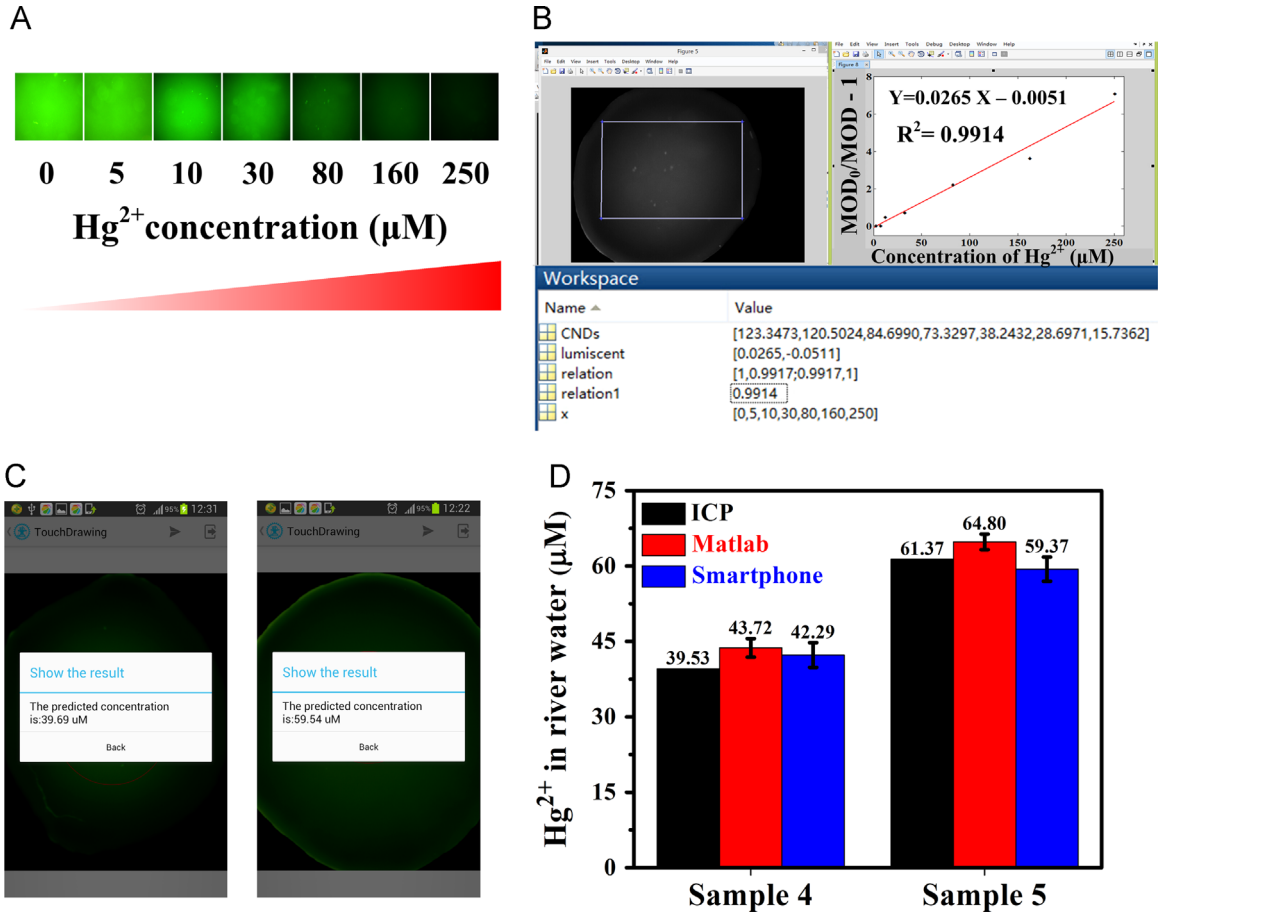

Fig. 5. Portable mercury ion sensing based on MATLAB code and smartphone APP. (A) Fluorescent images of water drops containing N-doped CNDs with different Hg^{2+} concentration; (B) the dependence of (MOD_0/MOD)-1 on concentrations of Hg^{2+} within the range of 5~250 μM; (C) quantification of Hg^{2+} by smartphone APP showing Hg^{2+} concentration in river water of 39.69 μM and 59.54 μM; (D) Hg^{2+} concentration in river water measured by MATLAB code (red), smartphone APP (blue) and ICP-AES (black). (For interpretation of the references to color in this figure legend, the reader is referred to the web version of this article.)

between contaminated and non-contaminated river water, providing the practical Hg^{2+} detection in river water.

3.5. Portable detection of Hg^{2+} based on programed MATLAB code and smartphone APP

Low concentrations of Hg^{2+} in the aqueous environment have been detected traditionally using expensive instruments, including AES, ICP-MS and AFS. However, these technologies are associated with limitations of high cost, large and un-portable. Therefore, there is still an unmet need for portable, low-cost and rapid Hg^{2+} detection based on imaging analysis. Fig. 5A presents the ROI images from water droplets with different Hg^{2+} concentrations (Fig. S10). It is clear that Hg^{2+} concentrations correlate with their brightness. To enable this colorimetric measurement portability and engineering for potential feasibility within smart phone, a MATLAB code to automatically analyze images and predict Hg^{2+} concentrations was developed. The MATLAB code can pick/read the grayscale value of image regions on smartphone. The quantification detection of Hg^{2+} concentration by using MATLAB code is shown in Fig. 5B. A linear relationship was found between MOD_0 /MOD-1 and Hg^{2+} concentration with $R^2=0.9914$. The output results via MATLAB code show that the predicted concentrations of river samples was 43.72 and 62.80 μM, which have a good match with the standard concentrations (39.53 and 61.37 μM) with a slight increase (5–8%), Figs. S11 and 5D. The MATLAB code for quantification of images would easily adapt to hardware changes from phone-to-phone (Wei et al., 2014). Furthermore, the cost of different Hg^{2+} detection method (including ICP-AES, PL spectrum and portable imaging analysis) is about 20, 25 and 5 dollar, respectively.

Smartphone conjunction with add-on devices, have shown great capability of data collection, analysis, display and sharing, making them suitable for point of care (POC) diagnostics (Xu et al., 2015). Hence, it is the first demonstration of the feasibility that POC quantification based on N-doped CNDs using smartphone APP, enabling portable, cost-effective and rapid Hg^{2+} detection as shown in Fig. 5C (**SI video file**). According to the fitting line (Fig. S12), the operational results show that the calculated concentration of river water is 42.29 and 69.37 μM, which have a good match with standard high concentrations (40 and 60 μM) with a slight increase (~10%), Fig. 5D**.** In the future, smartphone-based POC detection using our N-doped CNDs may offer a powerful and inexpensive method in aqueous environment monitoring and food safety analysis.

Supplementary material related to this article can be found online at http://dx.doi.org/10.1016/j.bios.2015.11.085

4. Conclusions

In summary, high-yield synthesis of N-doped CNDs ($38.4 \pm 3.4\%$) derived from hydrosoluble chitosan were developed, making it possible to produce N-doped CNDs in a large-scale manner. The nitrogen in biomass was incorporated in the CNDs in terms of N-C_3 (10%), pyridinic-like N (67%) and NH_2 (23%) respectively, which boosted the QY to 31.8%. The N-doped CNDs could serve as biocompatible fluorescence probes for multicolor live cell imaging. Also it serves as a biocompatible probe for sensitive detection of Hg^{2+} ions and detection limit of 80 nM. It could quantify Hg^{2+} concentration by portable MATLAB code and smartphone APP in river water, respectively. A high-yield synthesis of N-doped CNDs with high QY would hold great promise for multicolor bioimaging, portable Hg^{2+} detection by laptop/smartphone and further allowing potential warning of mercury ions contamination.

Acknowledgments

The authors thank the financial support from National Natural Science Foundation of China (51372051, 51321061), National Basic Science Research Program (2012CB339300), State Key Laboratory of Urban Water Resource and Environment of Harbin Institute of Technology (2013TS09), Innovation Talents of Harbin Science and Engineering (2013RFLXJ023) and Fundamental Research Funds for Central Universities (HIT.IBRSEM.201302). F.X. was supported by the Major International Joint Research Program of China (No. 11120101002) and International Science & Technology Cooperation Program of China (No. 2013DFG02930). The authors also thank Richard M. Laine of University of Michigan for his revision comments and improving English language.

Appendix A. Supplementary material

Supplementary data associated with this article can be found in the online version at http://dx.doi.org/10.1016/j.bios.2014.05.063.

References

Barati, A., Shamsipur, M., Abdollahi, H., 2015. Hemoglobin detection using carbon dots as a fluorescence probe. Biosens. Bioelectron. 71, 470–475.
Dong, Y., Pang, H., Yang, H.B., Guo, C., Shao, J., Chi, Y., Li, C.M., Yu, T., 2013. Carbon-based dots co-doped with nitrogen and sulfur for high quantum yield and excitation-independent emission. Angew. Chem. Int. Ed. 52 (30), 7800–7804.
Falco, C., Baccile, N., Titirici, M.M., 2011. Morphological and structural differences between glucose, cellulose and lignocellulosic biomass derived hydrothermal carbons. Green Chem. 13 (11), 3273–3281.
Gao, Z., Wang, L.B., Su, R.X., Huang, R.L., Qi, W., He, Z.M., 2015. A carbon dot-based "off-on" fluorescent probe for highly selective and sensitive detection of phytic acid. Biosens. Bioelectron. 70, 232–238.
Gu, J.J., Hu, D.H., Wang, W.N., Zhang, Q.H., Meng, Z., Jia, X.D., Xi, K., 2015. Carbon dot cluster as an efficient "off-on" fluorescent probe to detect Au(III) and glutathione. Biosens. Bioelectron. 68, 27–33.
Guo, Y.M., Wang, Z., Shao, H.W., Jiang, X.Y., 2013. Hydrothermal synthesis of highly fluorescent carbon nanoparticles from sodium citrate and their use for the detection of mercury ions. Carbon 52, 583–589.
Hsu, P.C., Chen, P.C., Ou, C.M., Chang, H.Y., Chang, H.T., 2013. Extremely high inhibition activity of photoluminescent carbon nanodots toward cancer cells. J. Mater. Chem. B 1 (13), 1774–1781.
Hsu, P.C., Shih, Z.Y., Lee, C.H., Chang, H.T., 2012. Synthesis and analytical applications of photoluminescent carbon nanodots. Green Chem. 14 (4), 917–920.
Hu, S., Trinchi, A., Atkin, P., Cole, I., 2015. Tunable photoluminescence across the entire visible spectrum from carbon dots excited by white light. Angew. Chem. Int. Ed. 54 (10), 2970–2974.
Jiang, K., Sun, S., Zhang, L., Lu, Y., Wu, A., Cai, C., Lin, H., 2015. Red, green, and blue luminescence by carbon dots: full-color emission tuning and multicolor cellular imaging. Angew. Chem. Int. Ed. 54 (18), 5360–5363.
Li, B.Q., Wang, L., Xu, F., Gang, X.M., Demirci, U., Wei, D.Q., Li, Y., Feng, Y.J., Jia, D.C., Zhou, Y., 2015. Hydrosoluble, UV-crosslinkable and injectable chitosan for patterned cell-laden microgel and rapid transdermal curing hydrogel in vivo. Acta Biomater. 22, 59–69.
Li, L.L., Ji, J., Fei, R., Wang, C.Z., Lu, Q., Zhang, J.R., Jiang, L.P., Zhu, J.J., 2012. A facile microwave avenue to electrochemiluminescent two-color graphene quantum dots. Adv. Funct. Mater. 22 (14), 2971–2979.
Liang, Q.H., Ma, W.J., Shi, Y., Li, Z., Yang, X.M., 2013. Easy synthesis of highly fluorescent carbon quantum dots from gelatin and their luminescent properties and applications. Carbon 60, 421–428.
Liu, R.H., Li, H.T., Kong, W.Q., Liu, J., Liu, Y., Tong, C.Y., Zhang, X., Kang, Z.H., 2013. Ultra-sensitive and selective Hg^{2+} detection based on fluorescent carbon dots. Mater. Res. Bull. 48 (7), 2529–2534.
Ma, Z., Ming, H., Huang, H., Liu, Y., Kang, Z.H., 2012. One-step ultrasonic synthesis of fluorescent N-doped carbon dots from glucose and their visible-light sensitive photocatalytic ability. New J. Chem. 36 (4), 861–864.
Park, S.Y., Lee, H.U., Park, E.S., Lee, S.C., Lee, J.W., Jeong, S.W., Kim, C.H., Lee, Y.C., Huh, Y.S., Lee, J., 2014. Photo luminescent green carbon nanodots from food-waste-derived sources: large-scale synthesis, properties, and biomedical applications. ACS Appl. Mater. Interfaces 6 (5), 3365–3370.
Sahu, S., Behera, B., Maiti, T.K., Mohapatra, S., 2012. Simple one-step synthesis of highly luminescent carbon dots from orange juice: application as excellent bio-imaging agents. Chem. Commun. 48 (70), 8835–8837.
Song, Y.C., Shi, W., Chen, W., Li, X.H., Ma, H.M., 2012. Fluorescent carbon nanodots conjugated with folic acid for distinguishing folate-receptor-positive cancer cells from normal cells. J. Mater. Chem. 22 (25), 12568–12573.

Sun, D., Ban, R., Zhang, P.H., Wu, G.H., Zhang, J.R., Zhu, J.J., 2013. Hair fiber as a precursor for synthesizing of sulfur- and nitrogen-co-doped carbon dots with tunable luminescence properties. Carbon 64, 424–434.
Sun, Y.P., Zhou, B., Lin, Y., Wang, W., Fernando, K.A.S., Pathak, P., Meziani, M.J., Harruff, B.A., Wang, X., Wang, H.F., Luo, P.J.G., Yang, H., Kose, M.E., Chen, B.L., Veca, L.M., Xie, S.Y., 2006. Quantum-sized carbon dots for bright and colorful photoluminescence. J. Am. Chem. Soc. 128 (24), 7756–7757.
Wang, J., Wang, C.F., Chen, S., 2012. Amphiphilic egg-derived carbon dots: rapid plasma fabrication, pyrolysis process, and multicolor printing patterns. Angew. Chem. Int. Ed. 51 (37), 9297–9301.
Wei, Q.S., Nagi, R., Sadeghi, K., Feng, S., Yan, E., Ki, S.J., Caire, R., Tseng, D., Ozcan, A., 2014. Detection and spatial mapping of mercury contamination in water samples using a smart-phone. Acs Nano 8 (2), 1121–1129.
Xu, X.Y., Akay, A., Wei, H.L., Wang, S.Q., Pingguan-Murphy, B., Erlandsson, B.E., Li, X. J., Lee, W., Hu, J., Wang, L., Xu, F., 2015. Advances in smartphone-based point-of-care diagnostics. Proc. IEEE 103 (2), 236–247.
Xu, Y., Wu, M., Liu, Y., Feng, X.Z., Yin, X.B., He, X.W., Zhang, Y.K., 2013. Nitrogen-doped carbon dots: a facile and general preparation method, photo-luminescence investigation, and imaging applications. Chemistry Eur. J. 19 (7), 2276–2283.
Zhang, J., Yuan, Y., Liang, G., Yu, S.-H., 2015. Scale-up synthesis of fragrant nitrogen-doped carbon dots from bee pollens for bioimaging and catalysis. Adv. Sci. 2 (4), 1500002.
Zhang, Y.Q., Ma, D.K., Zhuang, Y., Zhang, X., Chen, W., Hong, L.L., Yan, Q.X., Yu, K., Huang, S.M., 2012. One-pot synthesis of N-doped carbon dots with tunable luminescence properties. J. Mater. Chem. 22 (33), 16714–16718.
Zheng, X.T., Ananthanarayanan, A., Luo, K.Q., Chen, P., 2015. Glowing graphene quantum dots and carbon dots: properties, syntheses, and biological applications. Small 11 (14), 1620–1636.
Zhou, L., Lin, Y.H., Huang, Z.Z., Ren, J.S., Qu, X.G., 2012. Carbon nanodots as fluorescence probes for rapid, sensitive, and label-free detection of Hg^{2+} and biothiols in complex matrices. Chem. Commun. 48 (8), 1147–1149.
Zhu, C., Zhai, J., Dong, S., 2012. Bifunctional fluorescent carbon nanodots: green synthesis via soy milk and application as metal-free electrocatalysts for oxygen reduction. Chem. Commun. 48 (75), 9367–9369.
Zhu, S.J., Meng, Q.N., Wang, L., Zhang, J.H., Song, Y.B., Jin, H., Zhang, K., Sun, H.C., Wang, H.Y., Yang, B., 2013. Highly photoluminescent carbon dots for multicolor patterning, sensors, and bioimaging. Angew. Chem. Int. Ed. 52 (14), 3953–3957.